J. Fluid Mech. (1998), *vol.* 362, *pp.* 273–295. Printed in the United Kingdom

Stability of interfacial waves in aluminium reduction cells

By P. A. DAVIDSON AND R. I. LINDSAY

Department of Engineering, University of Cambridge, Trumpington Street, Cambridge CB2 1PZ, UK

(Received 11 June 1996 and in revised form 1 October 1997)

We investigate the stability of interfacial waves in conducting fluids under the influence of a vertical current density, paying particular attention to aluminium reduction cells in which such instabilities are commonly observed. We develop a wave equation for the interface in which the Lorentz force is expressed explicitly in terms of the fluid motion. Our wave equation differs from previous models, most notably that developed by Urata (1985), in that earlier formulations rested on a more complex, implicit coupling between the fluid motion and the Lorentz force. Our formulation furnishes a number of quite general stability results without the need to resort to Fourier analysis. (The need for Fourier analysis typifies previous studies.) Moreover, our equation supports both travelling and standing waves. We investigate each in turn.

We obtain three new results. First, we show that travelling waves may become unstable in the presence of a uniform, vertical magnetic field. (Our travelling waves are quite different to those discovered by previous investigators (Sneyd 1985 and Moreau & Ziegler 1986) which require more complex magnetic fields to become unstable.) Second, in line with previous studies we confirm that standing waves may also become unstable. In this context we derive a simple energy criterion which shows which types of motion may extract energy from the background magnetic field. This indicates that a rotating, tilted interface is particularly prone to instability, and indeed such a motion is often seen in practice. Finally, we use Gershgorin's theorem to produce a sufficient condition for the stability of standing waves in a finite domain. This allows us to place a lower bound on the critical value of the background magnetic field at which an instability first appears, without solving the governing equations of motion.

1. Introduction

Aluminium is produced by electrolysis in Hall–Heroult reduction cells. These cells consist of large carbon blocks (electrodes), between which lie a shallow layer of liquid aluminium together with a second layer of electrolyte (called cryolite). Unwanted disturbances are readily triggered at the cryolite–aluminium interface. (See figure 1.) In essence, these are long-wavelength interfacial gravity waves, modified by the intense magnetic and electric fields which pervade the cell. Under certain conditions these disturbances are observed to grow, disrupting the operation of the cell.

A somewhat simplified model of a cell is shown in figure 1. A large vertical current, perhaps 200–300 kA, flows downward from the carbon anode, passing through the electrolyte and aluminium layers before being collected in carbon cathode blocks at the base of the cell. The liquid layers are broad and shallow, perhaps 4 m $\times$ 10 m in plan, yet only 5–25 cm in depth. As we shall see, this large aspect ratio plays a central

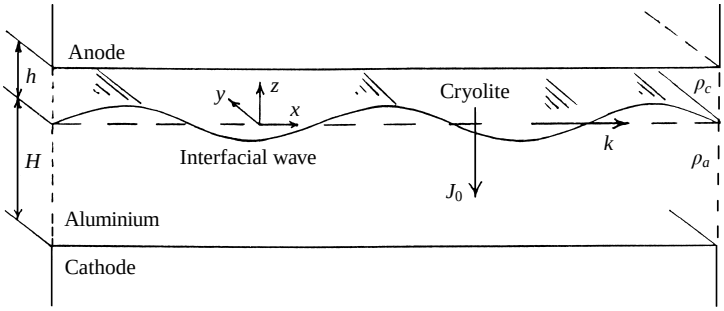

FIGURE 1. The cell geometry.

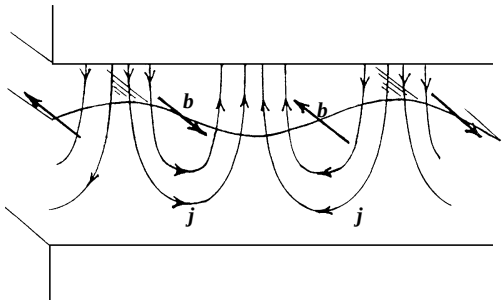

FIGURE 2. The perturbation in current and magnetic field.

role in the instability. In particular, it takes only a slight tilting of the interface to produce a substantial redistribution of current in the cell.

The second thing which strongly influences dynamics of the interface is the electrical conductivity of the materials involved. The aluminium is an excellent conductor, the carbon a moderate conductor, and the cryolite a very poor conductor. This ordering of the conductivities is critical to the way in which the current redistributes within the cell following a movement of the interface. It also explains why the fluid layers are kept so shallow. Most of the electrical power consumed by the cell is lost to Ohmic heating of the highly resistive electrolyte.

The earliest attempts to characterize these interfacial instabilities date back to the papers of Sele (1977) and of Urata (1985). These authors noticed that a displacement of the interface inevitably leads to a redistribution of current, $\boldsymbol{J}$, within the cell. This is illustrated in figure 2 where the perturbation in current, $\boldsymbol{j}$, is shown. In effect, excess current is drawn into the aluminium at those points where the thickness of the highly resistive cryolite is reduced, and less current is drawn at points where the cryolite depth is increased. The resulting perturbation in current is as shown, downward at the wave crests and upward at the valleys. Since the carbon cathode is much more resistive than the aluminium, these perturbations in vertical current feed into the aluminium but do not penetrate the cathode. Associated with $\boldsymbol{j}$ there is a perturbation in the magnetic field, $\boldsymbol{b}$, which is directed parallel to the wave crests. If $\boldsymbol{J}_0$ and $\boldsymbol{B}_0$ are the unperturbed current density and magnetic fields, then movement of the interface produces a perturbation in the Lorentz force given by $\boldsymbol{J}_0 \times \boldsymbol{b} + \boldsymbol{j} \times \boldsymbol{B}_0$.

Of course, the key question is whether or not this perturbation in force acts to reinforce the initial disturbance. This question was clarified, for cases where the lateral boundaries of the cell are ignored, by Sneyd (1985, 1992), Moreau & Ziegler (1986), and Pigny & Moreau (1992). These authors considered the (infinite) interface to be

perturbed by *travelling waves*. They found that the redistribution in current could combine with certain gradients in $\boldsymbol{B}_0$, particularly horizontal gradients in the vertical field, B_z, to cause an instability. The dominant physical mechanism underlying this phenomenon was identified by Davidson (1994).

These travelling-wave models have one serious drawback: they leave open the question of the influence of the lateral boundaries of the cell. This is particularly important as the waves observed in practice have wavelengths comparable with the lateral dimensions of the cell.

The *standing-wave* problem has recently been tackled by Sneyd & Wang (1994), Bojarevics & Romerio (1994), and, to a lesser extent, by Segatz & Droste (1994). Although these papers look, at first glance, rather different, the substance of their arguments is quite similar. They conclude that the stability characteristics of standing waves are very different to those of the travelling waves investigated earlier. Consequently, the papers by Sneyd & Wang and Bojarevics & Romerio represent a quite new insight into the phenomenon of cell stability. (We shall make frequent reference to these papers, so it is convenient to label them as SW94 and BR94.)

Both of the papers start by noting that, in the absence of a magnetic field, the interface may support an infinite number of conventional standing waves. The normal modes associated with these gravitational waves form an orthogonal set of functions, so that one can represent an arbitrary disturbance of the interface as the superposition of many such gravitational modes. When the Lorentz forces are neglected, these modes are, of course, decoupled. However, when the Lorentz forces are taken into account, certain gravitational modes are coupled. That is, the redistribution of current caused by one gravitational mode gives rise to a perturbed Lorentz force which, when Fourier-decomposed, can excite many other gravitational modes. When the magnetic field is large enough, this coupling leads to an instability, involving two or more adjacent gravitational frequencies.

The onset of instability was identified in SW94 and BR94 by the following method. First, they established a coupled set of equations of the form

$$\ddot{\boldsymbol{x}} + \boldsymbol{\Omega x} = \epsilon \boldsymbol{K x}. \tag{1.1}$$

Here $\boldsymbol{x}$ is a column vector which represents the amplitudes of the gravitational modes. The matrix $\boldsymbol{\Omega}$ is diagonal with elements equal to the square of the gravitational frequencies, and $\boldsymbol{K}$ is the interaction matrix which arises from the Lorentz force. The scalar ϵ is some dimensionless measure of this force. For example, ϵ may be the ratio of $J_0 B_0$ to inertia.

All of the coupling arises from $\boldsymbol{K}$. Its columns are determined by calculating the redistribution of current caused by one gravitational mode, evaluating the associated Lorentz force and then Fourier decomposing this force into components. We might refer to (1.1) as representing a Fourier or 'mode-by-mode' analysis of the problem.

These coupled equations represent an eigenvalue problem for the square of the natural frequencies. As noted in BR94, $\boldsymbol{K}$ is skew-symmetric, so the eigenvalues need not be real. In general there is a critical value of ϵ at which complex eigenvalues appear, representing instability.

A key point noted in both papers, but particularly emphasized in BR94, is that the dominant contribution to the perturbed Lorentz force arises from the interaction between a horizontal flow of current in the aluminium and the vertical component of the background magnetic field, B_z. The predictions of SW94 and BR94 are quite different to those of the earlier travelling-wave models. That is, standing waves are predicted to go unstable once B_z exceeds some critical value. Travelling waves, on the

other hand, are unstable whenever there is a horizontal gradient in B_z, provided, of course, that friction is ignored. The difference in these stability criteria suggests that the physical origins of the two types of instability are distinct.

Our paper falls into two parts. The first half focuses on the mechanisms of the instability. We start with a simple mechanical analogue which captures all the essential features of the instability. Next we derive a (wave-like) partial differential equation for the interface in which the Lorentz force is expressed directly in terms of the interfacial movement. By dispensing with the mode-by-mode analysis of SW94 and BR94, we arrive at a more compact description of the dynamics. This new equation allows us to identify the physical origin of the instability and to derive a simple energy criterion which shows which types of motion may extract energy from the Lorentz forces. On route, we show that the instability is not restricted to standing waves but may manifest itself in travelling waves and that these travelling waves are different to those studied before.

In the second half of this paper, we return to the Fourier approach of SW94 and BR94. (Equation (1.1) follows directly from our wave equation.) The key finding here is that a sufficient condition for stability can be obtained without the need to solve the equations of motion. Rather, Gershgorin's theorem can be used to establish a stability criterion. This allows us to place a lower bound on the critical value of the background magnetic field at which an instability first appears.

2. Simplifying assumptions and governing equations

Our simplified model of the cell is shown in figure 1. The undisturbed depths of cryolite and aluminium are h and H, and the unperturbed current flow is purely vertical and has magnitude J_0. We use a Cartesian coordinate system, (x, y, z), where z is vertical and directed upward. The origin for z lies at the undisturbed interface. On occasion we shall refer to cells which are rectangular in plan view, and these are given dimensions L_x and L_y. However, much of the analysis is can be applied to any shape of cell. The undisturbed interface is taken to be flat.

In accordance with experimental observations, we take the characteristic time-scale for the wave motion to be much greater than the diffusion time of the magnetic field. That is, we make the pseudo-static approximation $\mu\sigma uh \ll 1$, where μ is the permeability, σ is the conductivity, and u is a typical velocity. Thus, each time the interface moves, the current immediately relaxes to a new equilibrium distribution. Ohm's law is then

$$\boldsymbol{J} = \sigma \boldsymbol{E} = -\sigma \nabla \Phi; \quad \nabla^2 \Phi = 0. \tag{2.1}$$

We are concerned only with linear stability, so we consider infinitesimal perturbations of the interface of the form

$$z_s = \eta(x, y, t); \quad \eta \ll h, H.$$

The corresponding distributions of $\boldsymbol{J}$ and $\boldsymbol{B}$ are

$$\boldsymbol{J} = \boldsymbol{J}_0 + \boldsymbol{j} = -J_0 \hat{\boldsymbol{e}}_z - \sigma \nabla \phi,$$
$$\boldsymbol{B} = \boldsymbol{B}_0 + \boldsymbol{b}.$$

The boundary conditions on $\boldsymbol{J}$ arise from the ranking of the conductivities discussed in §1. That is,

$$\sigma_a \gg \sigma_{carbon} \gg \sigma_c. \tag{2.2}$$

Here the subscripts 'a' and 'c' refer to the aluminium and cryolite. It is not difficult to show (see Davidson 1994) that (2.2) requires $\phi_c = 0$ on $z = h$ and $\partial\phi_a/\partial z = 0$ on $z = -H$. Here ϕ is the perturbation in the electrostatic potential. The first of the boundary conditions states that the anode potential is fixed, while the second ensures that $\boldsymbol{j}$ does not penetrate into the cathode blocks. The boundary conditions at the interface are also discussed in Davidson (1994). They are continuity of normal current and the jump condition $\phi_c - \phi_a = (\sigma_a^{-1} - \sigma_c^{-1})J_0\eta$.

Like SW94 and BR94, we shall assume that the fluid is inviscid, that surface tension can be ignored, and that there is no background motion in the unperturbed state. The first of these assumptions means that our equations of motion cannot mimic the damping of high-wavenumber perturbations which occurs in practice. To compensate for this, we follow SW94 and BR94 and simply ignore those modes whose wavelengths are shorter than a certain (small but arbitrary) value.

The last of the three assumptions above (i.e. $\boldsymbol{u}_0 = 0$) greatly simplifies the stability analysis. Indeed, the inclusion of background motion increases the complexity of the problem to the level where analytical methods probably cease to be useful and a numerical approach is required. That is, the background flow must be calculated for each distribution of $\boldsymbol{J}_0 \times \boldsymbol{B}_0$, which in turn requires the introduction of some dissipation model. Moreover, terms like $\boldsymbol{u}_0 \cdot \nabla \boldsymbol{u}$ must be retained in the stability analysis which, in view of the complexity of $\boldsymbol{u}_0$, makes the subsequent analysis difficult. In line with previous investigations, therefore, we chose $\boldsymbol{u}_0$ to be zero although it is clear that this is not the case in a real cell. However, this simplification does severely limit the allowable distributions of $\boldsymbol{B}_0$. That is, to ensure that we are perturbing about an equilibrium configuration, we must satisfy $\nabla \times (\boldsymbol{J}_0 \times \boldsymbol{B}_0) = 0$. Given our assumed distributions of $\boldsymbol{J}_0$, we require $\boldsymbol{B}_0$ to be of the form

$$\boldsymbol{B}_0 = (B_x(x, y), B_y(x, y), B_z), \tag{2.3}$$

where B_z is spatially uniform. We shall assume that all three components of $\boldsymbol{B}_0$ are of the same order of magnitude. From Amperes law, $\nabla \times \boldsymbol{B} = \mu \boldsymbol{J}$, this implies that $B_x \sim B_y \sim B_z \sim \mu J_0 L$ where L is a typical lateral dimension.

We shall also follow SW94 and BR94, and indeed all other previous investigations, in assuming that the lateral boundaries of the cell are solid and impermeable. In fact, this is often not the case, but it does seem like a reasonable starting place.

Our final assumption relates to the aspect ratio of the liquid layers. We shall assume that $kh \ll 1$, where k is a typical wavenumber. In effect, we use the shallow-water approximation. This leads directly to a number of simplifying features, many of which are noted in either SW94 or else in BR94. At this point we shall simply state these simplifications. Later, in §4, we confirm that each of these simplifications is indeed valid. In the meantime, we merely note that, as a result of the shallow-water approximation, and to leading order in kh, it may be shown that:

(*a*) $\boldsymbol{j}$ is vertical in the cryolite;
(*b*) $\boldsymbol{j}$ is horizontal in the aluminium and is uniformly distributed across that layer;
(*c*) the perturbed Lorentz force acting on the cryolite may be neglected;
(*d*) the velocity in each layer is uniform in z and horizontal;
(*e*) the dominant contribution to the perturbed Lorentz force in the aluminium is $\boldsymbol{j} \times (B_z \hat{\boldsymbol{e}}_z)$.

In fact, it is not difficult to see how these simplifications arise. Consider the situation shown in figure 3, where the disturbance has a long wavelength. Approximations (*a*) and (*b*) are purely geometric and are a consequence of the ranking of the conductivities. That is, the dominant resistance to the flow of current is the thin sheet

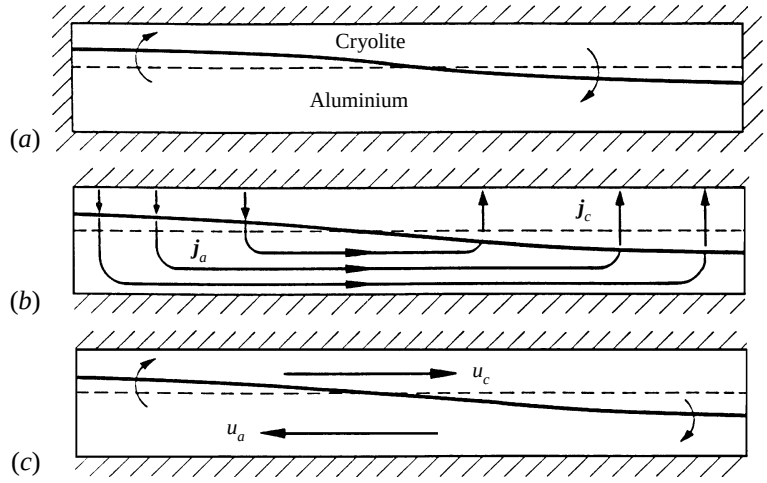

FIGURE 3. A long-wavelength disturbance of the interface results in a perturbed current flow, $\boldsymbol{j}$, which is largely vertical in the cryolite and horizontal in the aluminium. It also results in a 'sloshing' motion in the two liquids which is largely horizontal.

of cryolite, so the current passes directly downward through this layer (condition (*a*)). The aluminium, which is a very good conductor, is almost an equipotential surface, so that spatial variations of J_z in the cryolite (due to undulations of the interface) lead to a 'shorting' of the perturbed current through the aluminium. This 'shorted' current is almost purely horizontal (condition (*b*)). The neglect of the perturbed Lorentz force in the cryolite (condition (*c*)) stems from the fact that $\boldsymbol{j}_c \ll \boldsymbol{j}_a$, which in turn arises from the aspect ratio $kh \ll 1$. The uniformity of the velocity in the two fluid layers (condition (*d*)) follows from the fact that the Lorentz force in the aluminium is independent of depth.

This leaves only simplification (*e*) to justify, and here there is some subtlety in the argument. Using subscripts H and V to indicate horizontal and vertical components of $\boldsymbol{J}$ and $\boldsymbol{B}$, it seems reasonable to neglect $\boldsymbol{j}_H \times \boldsymbol{B}_H$ and $\boldsymbol{j}_V \times \boldsymbol{B}_H$ because the former is vertical and so merely perturbs the vertical pressure gradient, while the latter is much smaller than $\boldsymbol{j}_H \times \boldsymbol{B}_V$, by virtue of (*b*). (Actually, $\boldsymbol{j}_H \times \boldsymbol{B}_H$ does cause some horizontal flow via the horizontal gradients in pressure. However, this is of order $(kH)\boldsymbol{j}_H \times \boldsymbol{B}_H$ and so is much less than $\boldsymbol{j}_H \times \boldsymbol{B}_V$.) Finally, the neglect of $\boldsymbol{b} \times \boldsymbol{J}_0$ relies on the fact that $\boldsymbol{b}$ is of order $\mu \boldsymbol{j}_H H$, while $\boldsymbol{B}_0$ is of order $\mu J_0 L_x$, so that $\boldsymbol{J}_0 \times \boldsymbol{b}$ is of order kH smaller than $\boldsymbol{j} \times \boldsymbol{B}_V$. Condition (*e*) was particularly emphasized in BR94.

As already noted, we shall justify conditions (*a*) to (*d*) in §4. Independent confirmation may be obtained by taking the limit $kH \to 0$ in the analysis of SW94, which provides an explicit proof of assumptions (*a*) to (*e*).

3. A mechanical analogue of interfacial instabilities

To provide some initial physical insight into reduction cell instabilities we look first at a simple mechanical analogue. This captures all the essential physics and points the way for the analysis of the more complex hydrodynamic problem.

Consider the compound pendulum shown in figure 4. It consists of a large flat aluminium plate attached to an adjacent, parallel surface by a light, rigid strut. The strut is pivoted at its top end so that the plate is free to swing about two horizontal

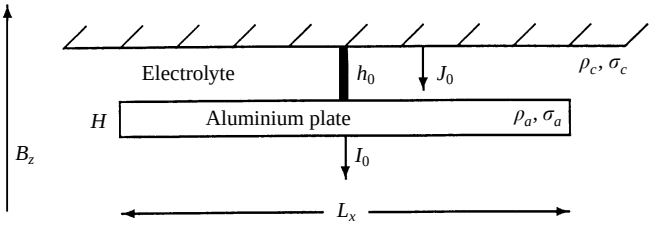

FIGURE 4. The compound pendulum.

axes, x and y. Let the plate have thickness H and lateral dimensions L_x, L_y. The gap h between the plate and the upper surface (which is an electrode) is filled with a weakly conducting electrolyte, and a uniform current, J_0, passes vertically downward through the electrolyte into the plate. This current generates a magnetic field which is predominantly horizontal. In addition, we impose a uniform, vertical magnetic field, B_z, as shown. The current which enters the plate from above must be withdrawn from the bottom of the plate. The manner in which this is achieved is unimportant, so we shall assume that the current flows horizontally to the centre of the plate where it is tapped off.

In line with the assumptions which we have made about the cell, we shall assume that the periods of oscillations are much greater than the diffusion time of the magnetic field, the conductivity of the aluminium is high enough for the plate to be treated as an equipotential surface, say $\Phi = 0$, and the plate and electrolyte layer are thin and broad ($L_x, L_y \gg h, H$). In addition, it is convenient (though strictly not necessary) to assume that $B_z \gg B_x, B_y$ so that we may ignore the Lorentz forces arising from B_x, B_y. Similarly, it is convenient to assume that the density of the electrolyte is much less than that of the plate, so that we may ignore the inertia of the electrolyte.

It is clear that we have replaced one mechanical system (the cell), which has an infinite number of degrees of freedom, with another which has only two degrees of freedom. However, the nature of the motion in the two cases is not dissimilar. In both systems, we have movement of the aluminium associated with a tilting of the electrolyte–aluminium interface. In a cell this takes the form of a sloshing back and forth of the aluminium as the interface tilts first one way and then the other (see figure 3).

Let θ_x and θ_y be the angles of rotation of the plate measured about the x- and y-axes, the origin of which lies at the centre of the electrolyte–plate interface. Also, let $h(x, y)$ be the local thickness of the electrolyte, Φ_0 be the electrode potential, which is fixed, and h_0 be the equilibrium value of h. Then, in the narrow gap approximation, we have

$$\Phi = \Phi_0 z/h; \quad h = h_0 + \theta_y x - \theta_x y.$$

Equation (2.1) now gives the perturbed current density in the electrolyte as

$$\boldsymbol{j}_c = [J_0(\theta_y x - \theta_x y)/h_0]\hat{\boldsymbol{e}}_z,$$

from which we may calculate the net flow of (perturbed) current within the plate:

$$\delta I_x = \frac{J_0 L_y \theta_y}{2h_0}\left[(L_x/2)^2 - x^2\right]; \quad \delta I_y = -\frac{J_0 L_x \theta_x}{2h_0}\left[(L_y/2)^2 - y^2\right]. \tag{3.1}$$

The resulting Lorentz force acting on the plate can now be calculated, and taking moments about the pivot, we obtain two equations of motion for the pendulum.

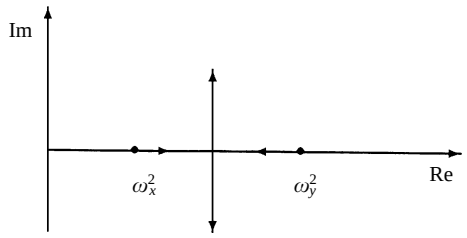

FIGURE 5. Variations of ω^2 with J_0B_z for the compound pendulum.

Setting $\gamma_x = \theta_x/L_x^2$ and $\gamma_y = \theta_y/L_y^2$ and using ω_x and ω_y to represent the conventional gravitational frequencies of the pendulum, we obtain

$$\ddot{\gamma}_x + \omega_x^2\gamma_x = -\left(J_0B_z/\rho_aH\right)\gamma_y, \tag{3.2a}$$

$$\ddot{\gamma}_y + \omega_y^2\gamma_y = \left(J_0B_z/\rho_aH\right)\gamma_x. \tag{3.2b}$$

Notice the similarity between (3.2) and (1.1). Notice also the skew symmetry in the coupling terms associated with the Lorentz forces. If we now let $\gamma \sim e^{j\omega t}$, it is easy to show that ω^2 is real for small values of J_0B_z and complex for large values of J_0B_z. The transition to instability occurs at

$$\frac{2J_0B_z}{\rho_aH} = \left|\omega_x^2 - \omega_y^2\right|. \tag{3.3}$$

We shall see that remarkably similar expressions determine the stability of the interface in a reduction cell.

The behaviour of ω^2 in the complex plane is shown schematically in figure 5. As J_0B_z is increased the two natural frequencies converge on the real axis. At a critical value of J_0B_z, given by (3.3), the two frequencies meet and then move off into the complex plane. Clearly, the sensitivity of the pendulum to the destabilizing influence of J_0B_z depends on the initial separation of the natural frequencies.

We may think of the Lorentz force as playing two roles. In the first instance it modifies the gravitational frequencies, pulling them together on the real axis. Once these frequencies coincide, so that the plate oscillates at the same frequency in two directions, the Lorentz force adopts a second role in which it supplies energy to the pendulum. Unstable motion then follows.

We may use a simple energy argument to show why, whenever the plate oscillates with a single frequency in two perpendicular directions, an instability is inevitable. From (3.1), the work done by the Lorentz force, $\delta\boldsymbol{F}\cdot\boldsymbol{u}$, is

$$\dot{W} = J_0B_zL_xL_y[L_y^2\theta_x\dot{\theta}_y - L_x^2\theta_y\dot{\theta}_x]/12. \tag{3.4}$$

Now suppose that θ_x and θ_y both oscillate at frequency ω, but are $\frac{1}{2}\pi$ out of phase. Then the time-averaged value of $\dot{W}$ is non-zero, implying unstable motion.

Physically, a tilting of the plate in one direction, say θ_x, produces a nearly horizontal flow of current in the aluminium which interacts with B_z to produce a horizontal force δF_x which is in-phase with θ_x. This tilting also produces a horizontal velocity, u_y, which is $\frac{1}{2}\pi$ out of phase with the force δF_x and mutually perpendicular to it. Two such tilting motions in perpendicular directions can reinforce each other, with the force from one doing work on the velocity of the other. This is, in effect, the instability mechanism.

Note that this *instability mechanism* is independent of the action of gravity. That is, provided the plate can oscillate at the same frequency in two directions, it will become unstable. (Circular and square plates are unstable at arbitrarily small values of B_z.) The *stability threshold*, on the other hand, does depend on gravity, in that it is dependent on the initial separation of the gravitational frequencies.

We shall see that the same distinction arises in reduction cells. That is, the point at which the interface becomes unstable depends on the initial separation of the gravitational frequencies for interfacial waves. This was established by SW94 and BR94. However, the instability mechanism (the mechanism by which unstable growth is maintained) does not depend on gravity. In fact, if our mechanical analogue is at all representative of interfacial instabilities, we would expect an instability to develop whenever the aluminium is free to slosh back and forth at a single frequency in two mutually perpendicular directions. We shall see that this often provides an accurate picture of the instability.

4. A generalized shallow-water equation for interfacial waves

We now derive a shallow-water equation for interfacial waves. This equation is more general than the 'mode-by-mode' description of (1.1) in that it makes no assumption regarding the existence or shape of lateral boundaries. Moreover, it is compact and so a physical interpretation of the instability is more readily obtained.

We start with conventional shallow-water theory. It is not difficult to show that, to second order in kH, the pressure in each layer is hydrostatic. As a consequence, we may apply the conventional shallow-water equation to each layer in turn. This is a two-dimensional, horizontal equation of motion:

$$\rho\frac{\mathrm{D}\boldsymbol{u}_H}{\mathrm{D}t} + \rho g\nabla H_a = -\nabla P_0 + \boldsymbol{F}_H.$$

(See Pedlosky (1979) for a formal justification of the shallow-water approximation when body forces are present.) Here $H_a(x, y)$ is the aluminium depth, P_0 is the interfacial pressure, and $\boldsymbol{F}_H$ is the horizontal body force in each layer. The unfamiliar term on the left arises from the horizontal gradient in pressure. Note that, since $\boldsymbol{F}_H$ is independent of z (to leading order in kH), this is a strictly two-dimensional equation. That is,

$$\boldsymbol{u} = \boldsymbol{u}_H(x, y) + O(kH); \quad \boldsymbol{u}_H = (u_x, u_y, 0).$$

We now linearize our equation of motion about a base state of zero background motion. Taking $H_a = H + \eta(x, y, t)$, we obtain

$$\rho\frac{\partial\boldsymbol{u}_H}{\partial t} + \rho g\nabla\eta = -\nabla P_0 + \boldsymbol{F}.$$

Although $\boldsymbol{u}_H$ is a two-dimensional velocity field, vertical movement of the interface means that the two-dimensional divergences of $\boldsymbol{u}_{aH}$ and $\boldsymbol{u}_{cH}$ are both non-zero. In fact, it is readily confirmed that

$$\nabla\cdot(H\boldsymbol{u}_a) = -\nabla\cdot(h\boldsymbol{u}_c) = -\frac{\partial\eta}{\partial t}.$$

(Here we have dropped the subscript H for convenience.) Next, we replace $\boldsymbol{u}_a$ and $\boldsymbol{u}_c$ by the volume fluxes $\boldsymbol{q}_a = H\boldsymbol{u}_a$ and $\boldsymbol{q}_c = -h\boldsymbol{u}_c$. Also, by virtue of condition (c) in §2, we may take $\boldsymbol{F}_c = 0$ (to leading order in kH). This is valid because, as we shall see, the current in the cryolite is an order of magnitude smaller than that in the

aluminium. Our governing equations now become

$$\frac{\rho_c}{h}\frac{\partial \boldsymbol{q}_c}{\partial t} - \rho_c g \nabla \eta = \nabla P_0, \tag{4.1}$$

$$\frac{\rho_a}{H}\frac{\partial \boldsymbol{q}_a}{\partial t} + \rho_a g \nabla \eta = -\nabla P_0 + \boldsymbol{F}_a, \tag{4.2}$$

$$\nabla \cdot \boldsymbol{q}_c = \nabla \cdot \boldsymbol{q}_a = -\frac{\partial \eta}{\partial t}. \tag{4.3}$$

We now perform a Helmholtz decomposition on $\boldsymbol{q}$:

$$\boldsymbol{q} = \boldsymbol{q}_R + \boldsymbol{q}_P.$$

That is, we divide $\boldsymbol{q}$ into a solenoidal, rotational part and an irrotational component of finite divergence. The boundary conditions on $\boldsymbol{q}_a$ and $\boldsymbol{q}_c$ are that $\boldsymbol{q} \cdot \boldsymbol{n}$ vanishes at the boundary, S. An appropriate decomposition is therefore

$$\nabla \times \boldsymbol{q}_P = 0, \quad \nabla \cdot \boldsymbol{q}_P = -\frac{\partial \eta}{\partial t}, \quad \boldsymbol{q}_P \cdot \boldsymbol{n} = 0 \quad \text{on} \quad S; \tag{4.4}$$

$$\nabla \times \boldsymbol{q}_R = \nabla \times \boldsymbol{q}, \quad \nabla \cdot \boldsymbol{q}_R = 0, \quad \boldsymbol{q}_R \cdot \boldsymbol{n} = 0 \quad \text{on} \quad = S. \tag{4.5}$$

(Note that the rotational and potential components of an equation may be equated. We shall use this later.) Evidently, $\boldsymbol{q}_R$ is zero in the electrolyte, while $\boldsymbol{q}_P$ is the same in both layers:

$$\boldsymbol{q}_c = \boldsymbol{q}_P; \quad \boldsymbol{q}_a = \boldsymbol{q}_P + \boldsymbol{q}_R.$$

We now rewrite (4.1) and (4.2) in terms of $\boldsymbol{q}_P$ and $\boldsymbol{q}_R$, eliminate P_0 by adding the equations, and use (4.4) to express η in terms of $\boldsymbol{q}_P$. The resulting equation of motion is

$$\bar{\rho}\frac{\partial^2 \boldsymbol{q}_P}{\partial t^2} - \Delta\rho g \nabla^2 \boldsymbol{q}_P = \frac{\partial \boldsymbol{F}_a}{\partial t} - \frac{\rho_a}{H}\frac{\partial^2 \boldsymbol{q}_R}{\partial t^2}, \tag{4.6}$$

where $\bar{\rho} = \rho_c/h + \rho_a/H$ and $\Delta\rho = \rho_a - \rho_c$. Note that, when the Lorentz force is zero, we recover the conventional equation for interfacial waves in the shallow-water limit:

$$\frac{\partial^2 \boldsymbol{q}_P}{\partial t^2} - c^2 \nabla^2 \boldsymbol{q}_P = 0, \quad c^2 = \Delta\rho g/\bar{\rho}. \tag{4.7}$$

We now evaluate $\boldsymbol{j}_a$, and hence $\boldsymbol{F}_a$, using the long-wavelength approximation of §2. In the cryolite we have, to leading order in kh, $\partial^2\Phi/\partial z^2 = 0$ from which

$$\Phi_c = \Phi_0 z/(h-\eta) + O(kh),$$
$$\boldsymbol{j}_c = -(J_0\eta/h)\hat{\boldsymbol{e}}_z + O(kh).$$

This current passes into the aluminium, and so the boundary conditions on $\boldsymbol{j}_{za}$ are

$$\boldsymbol{j}_{za} = -(J_0\eta/h)\hat{\boldsymbol{e}}_z \quad \text{on} \quad z = 0;$$
$$\boldsymbol{j}_{za} = 0 \quad \text{on} \quad z = -H.$$

It is readily confirmed (by direct substitution) that the conditions of zero divergence and zero curl, as well as the boundary conditions given above, are satisfied by

$$\boldsymbol{j}_a = \boldsymbol{j}_H(x,y) - (1 + z/H)(J_0\eta/h)\hat{\boldsymbol{e}}_z.$$

Here $\boldsymbol{j}_H$ is the horizontal component of the current density in the aluminium which

satisfies

$$\nabla \times \boldsymbol{j}_H = 0, \quad \nabla \cdot \boldsymbol{j}_H = \frac{J_0 \eta}{Hh}, \quad \boldsymbol{j}_H \cdot \boldsymbol{n} = 0 \quad \text{on} \quad S. \tag{4.8}$$

(This expression for $\boldsymbol{j}_a$ looks different to those derived in BR94 and SW94, but it is readily confirmed that they are identical in the limit $kH \to 0$.) Comparing (4.8) with (4.4) we find

$$\frac{\partial \boldsymbol{j}_H}{\partial t} = -\frac{J_0}{hH} \boldsymbol{q}_P. \tag{4.9}$$

This is the key relationship which allows us to express the Lorentz force in terms of the fluid motion and therefore deserves some special attention. It is equivalent to (3.1) which relates the current, and hence the Lorentz force, to the motion of the pendulum. The physical basis of (4.9) is contained in figure 3. When the interface tilts, there is a horizontal flow of current from the high to the low side of the interface. Simultaneously, there is a horizontal rush of aluminium in the opposite direction. It is this coupling which lies at the heart of the instability, and which is expressed by (4.9).

We now invoke condition (*e*) of §2 which states that the leading term in the Lorentz force arises from the background component of B_z. Substituting for $\boldsymbol{F}_a$ in (4.6) gives

$$\frac{\partial^2 \boldsymbol{q}_P}{\partial t^2} - c^2 \nabla^2 \boldsymbol{q}_P = \frac{J_0 B_z}{\bar{\rho} hH} \hat{\boldsymbol{e}}_z \times \boldsymbol{q}_P - \frac{1}{\bar{\rho}} \frac{\partial \boldsymbol{F}_R}{\partial t}. \tag{4.10}$$

Here $\boldsymbol{F}_R$ is the rotational part of $\boldsymbol{F}_a$, which satisfies

$$\nabla \cdot \boldsymbol{F}_R = 0, \quad \boldsymbol{F}_R \cdot \boldsymbol{n} = 0 \quad \text{on} \quad S. \tag{4.11}$$

Note that $\boldsymbol{F}_R$, like $\boldsymbol{q}_R$, integrates to zero throughout the fluid volume, V. Introducing

$$\omega_B^2 = J_0 B_z / \bar{\rho} hH,$$

we might rewrite (4.10) in the more compact form

$$\frac{\partial^2 \boldsymbol{q}_P}{\partial t^2} - c^2 \nabla^2 \boldsymbol{q}_P = \omega_B^2 [\hat{\boldsymbol{e}}_z \times \boldsymbol{q}_P]_P. \tag{4.12}$$

The subscript P on the bracket implies that we take only the irrotational component of $\hat{\boldsymbol{e}}_z \times \boldsymbol{q}_P$. (The boundary condition on the decomposition follows from (4.11).) This wave equation differs from previous shallow-water descriptions of the interfacial waves in that we have expressed the Lorentz force explicitly in terms of the motion.

There are many simplifications embedded in (4.12) which result from the shallow-water approximation, $kh \ll 1$. In order to confirm that we have been consistent throughout, we have generalized the analysis to arbitrary values of kh and then taken the limit of small kh. Once again, we arrive at (4.12). Independent confirmation of (4.12) is provided by SW94. Specifically, when (4.12) is rewritten in matrix form and applied to a rectangular boundary, the results are identical to those of SW94 in the limit of small kh. (See §6.)

Finally, to obtain the most compact version of our wave equation, it is convenient to introduce potentials for $\boldsymbol{q}_P$ and $\boldsymbol{F}_P = \boldsymbol{F}_a - \boldsymbol{F}_R$:

$$\boldsymbol{q}_P = \nabla \phi_P, \quad \frac{\partial \boldsymbol{F}_P}{\partial t} = \bar{\rho} \omega_B^2 \nabla \Psi.$$

Then (4.12) becomes

$$\frac{\partial^2 \phi_P}{\partial t^2} - c^2 \nabla^2 \phi_P = c^2 k_B^2 \Psi; \quad \nabla^2 \Psi = 0, \tag{4.13}$$

where k_B is defined as ω_B/c. The corresponding boundary conditions on ϕ_P and Ψ are

$$\nabla\phi_P \cdot \boldsymbol{n} = 0, \quad \nabla\Psi \cdot \boldsymbol{n} = (\nabla\phi_P \times \boldsymbol{n})_z. \tag{4.14}$$

Note that the boundary condition on Ψ comes directly from (4.10) and from the definition of $\boldsymbol{F}_P$.

5. General properties of the governing PDE

The shallow-water equation (4.12) supports both travelling waves and standing waves. As a prelude to our discussion of instabilities in closed, rectangular domains, it seems appropriate to examine the general properties of (4.12) and (4.13). We shall show that both travelling and standing waves may become unstable, and that the unstable travelling waves are quite different to those studied previously. We also derive an energy criterion for instability. Finally, we look at circular domains as these manifest the instability in its purest form.

5.1. *Travelling waves*

Perhaps the simplest geometry to consider is an infinitely long channel of width L, say $0 < x < L$. The easiest way of identifying travelling waves is to write both Ψ and ϕ_P in the form

$$\phi_P = \hat{\phi}(x)\exp[\mathrm{j}(\omega t - k_y y)]$$

and define a second wavenumber, k_x, through the expression

$$k_x^2 = \omega^2/c^2 - k_y^2.$$

Then (4.13) gives the eigenvalue problem

$$\hat{\phi}'' + k_x^2\hat{\phi} = -k_B^2\hat{\Psi}, \qquad \frac{\partial\hat{\phi}}{\partial x} = 0 \quad \text{on} \quad x = 0, L;$$

$$\hat{\Psi}'' - k_y^2\hat{\Psi} = 0, \qquad \frac{\partial\hat{\Psi}}{\partial x} = jk_y\hat{\phi} \quad \text{on} \quad x = 0, L.$$

The solution for $\hat{\phi}$ is

$$\hat{\phi} = -\frac{k_B^2\hat{\Psi}(0)}{k_x^2 + k_y^2}[\cosh k_y x + B\sinh k_y x + C\cos k_x x + D\sin k_x x],$$

where the four boundary conditions not only define B, C, and D, but also lead to a dispersion relationship for k_x in the form

$$2(k_B L)^4\left[\cosh q\cos p - 1 + \tfrac{1}{2}\left(p/q - q/p\right)\sinh q\sin p\right] + \left(p^2 + q^2\right)^2\left(p/q\right)\sinh q\sin p = 0, \tag{5.1}$$

where $p = k_x L$ and $q = k_y L$. When the Lorentz forces are zero ($k_B = 0$), this gives $k_x = m\pi/L$, which represents conventional travelling waves in a channel. For a finite value of k_B, and for an arbitrary wavenumber, k_y, we can always find a solution of (5.1) for which k_x is real. This represents stable travelling waves.

However (5.1) also supports unstable waves. That is, for real values of k_B and k_y, we can find complex values of k_x which satisfy (5.1). This leads to complex frequencies and therefore to unstable motion. Figure 6 shows the neutral stability curve for waves in the range $0 < q < 10$. Note that these unstable travelling waves are quite distinct

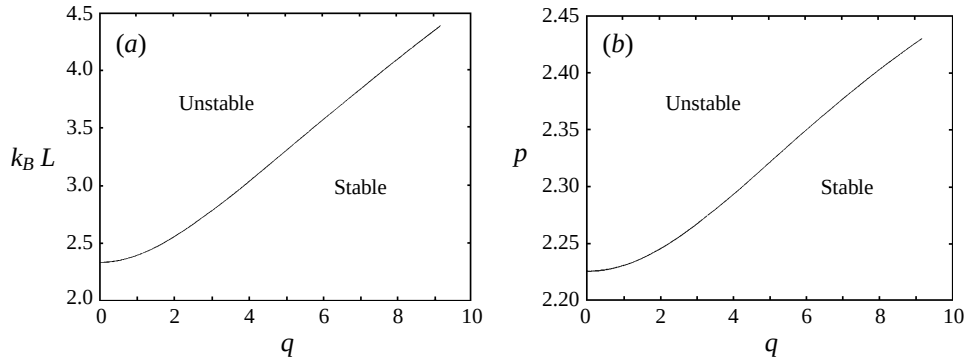

FIGURE 6. Neutral stability curves corresponding to (5.1).

from those identified in previous studies. Specifically, our travelling waves require only a uniform B_z to sustain unstable growth and vanish, or become stable, when the boundaries are removed.

5.2. *An energy criterion for instability*

We now turn our attention to closed domains. We start by noting that the coupling between the components of $\boldsymbol{q}_P$ is skew-symmetric. It is precisely this skew-symmetry which gives rise to the instability of the pendulum. A hint as to the significance of this skew-symmetry comes from integrating (4.12) over V. Let $\boldsymbol{Q}$ be the global linear momentum of the aluminium:

$$\boldsymbol{Q} = \int \boldsymbol{q}_a \mathrm{d}V = \int \boldsymbol{q}_P \mathrm{d}V.$$

Then integrating (4.10) gives

$$\frac{\partial^2 \boldsymbol{Q}}{\partial t^2} - c^2 \int \nabla^2 \boldsymbol{q}_P \mathrm{d}V = \omega_B^2 (\hat{\boldsymbol{e}}_z \times \boldsymbol{Q}). \tag{5.2}$$

Now suppose that ω_B is large enough for the Lorentz force to dominate the gravitational forces. That is, $\omega_B^2 \gg c^2 k^2$, where k is the dominant wavenumber of the disturbance. Then (5.1) simplifies to

$$\frac{\partial^2 \boldsymbol{Q}}{\partial t^2} \approx \omega_B^2 (\hat{\boldsymbol{e}}_z \times \boldsymbol{Q}) \quad (\omega_B \gg ck)$$

from which

$$\frac{\partial^4 \boldsymbol{Q}}{\partial t^4} \approx -\omega_B^4 \boldsymbol{Q} \quad (\omega_B \gg ck). \tag{5.3}$$

Equation (5.3) gives rise to complex wave frequencies, and so we would expect that a disturbance with non-zero linear momentum, $\boldsymbol{Q}$, will become unstable for sufficiently large values of $J_0 B_z$. We shall confirm later, by numerical experiment, that this is indeed the case.

We now pose the question: how is the instability maintained? We would like to establish an equation like (3.5) which identifies the source of energy for the instability. Once again, our wave equation (4.12) provides a convenient way forward. We take the dot product of (4.10) with $\boldsymbol{q}_P$, use (4.4) to relate $\nabla \cdot \boldsymbol{q}_P$ to η, and integrate over V

while noting that $\boldsymbol{q}_P \cdot \boldsymbol{F}_R$ integrates to zero. This gives

$$\frac{\partial}{\partial t}\int \left[\tfrac{1}{2}\bar{\rho}\dot{\boldsymbol{q}}_P^2 + \tfrac{1}{2}\Delta\rho g\dot{\eta}^2\right] \mathrm{d}V = \frac{J_0 B_z}{hH}\int (\boldsymbol{q}_P \times \dot{\boldsymbol{q}}_P)_z \,\mathrm{d}V. \tag{5.4}$$

For the oscillation to grow, the integral on the left must increase with time, so, if the right-hand integral is positive definite, the motion will be unstable. Now our simple analogue of a compound pendulum suggests that the interface will be unstable whenever the aluminium is free to slosh back and forth in two mutually perpendicular directions and at a single frequency. That is, the cell will be unstable whenever the geometry of the cell admits modes of the form

$$\boldsymbol{q}_P = \big(q_x(x)\cos\omega t, q_y(y)\sin\omega t\big) \tag{5.5}$$

where q_x and q_y are both positive. It is readily confirmed that this is indeed the case since in such instances the integral on the right of (5.4) becomes

$$\int (\boldsymbol{q}_P \times \dot{\boldsymbol{q}}_P)_z \,\mathrm{d}V = \omega \int q_x q_y \mathrm{d}V > 0 \tag{5.6}$$

and instability follows. Note that (5.5) corresponds to a pseudo-rotating vector and thus to a tilted interface which is executing a pseudo-rotational motion. Such a rotating interface is frequently associated with reduction cell instabilities (Segatz & Droste 1994).

The physical reasons for this instability are precisely the same as for the compound pendulum. They are implied in figure 3 and bound up in equation (4.9). A tilting of the interface in one direction causes a horizontal flow of current and of aluminium. The interaction of this current with B_z produces a horizontal force which is mutually perpendicular to, and $\frac{1}{2}\pi$ out of phase with, the horizontal motion in the aluminium. Two such tilting motions in perpendicular directions can reinforce each other, with the force from one motion acting on the velocity field of the other.

Of course, we have not determined which geometries admit modes of the form (5.5). However, there are at least two simple cases in which (5.5) constitutes a valid mode: these are square and circular domains in the limit of small ω_B/ω. (The circular case is analysed below.) In general, though, for rectangular cells of arbitrary aspect ratio, (5.5) is not a valid mode. Nevertheless (5.4) remains valid. That is, equation (5.4) represents a simple energy criterion which shows which type of wave motion may extract energy from the electric and magnetic fields. If the interface is to be unstable, we simply require

$$\int (\boldsymbol{q}_P \times \dot{\boldsymbol{q}}_P)_z \mathrm{d}V > 0. \tag{5.7}$$

Conversely, a given mode $\boldsymbol{q}_P^*$ cannot destabilize a cell if $\int (\boldsymbol{q}_P^* \times \dot{\boldsymbol{q}}_P^*)_z \mathrm{d}V < 0$. This is true whether or not $\boldsymbol{q}_P^*$ is a solution of (4.12).

Note that our description of the *instability mechanism* does not involve gravity. It is purely electromagnetic in its origin. The role of gravity is simply to provide an equilibrium configuration about which we may perturb. However, gravity does influence the *stability threshold*. This is because, in order to satisfy (5.7), our interface must be able to support two mutually perpendicular oscillations at the same frequency. When ω_B is weak, this need not be the case. As with the compound pendulum, the first role of B_z is to shift the position of the gravitational frequencies on the real axis until two frequencies meet. Expression (5.7) does not help therefore with determining the stability threshold.

5.3. *Instabilities in circular domains*

We conclude this section by looking at unstable waves in closed, circular domains. This is of interest as it demonstrates the instability in a particularly simple way. Suppose the fluids occupy the domain $0 < r < R$, and consider solutions of the form

$$\phi_P = \hat{\phi}(r)\exp[\mathrm{j}(\theta - \omega t)]; \quad \Psi = \hat{\Psi}(r)\exp[\mathrm{j}(\theta - \omega t)].$$

It is readily confirmed that (4.13) requires $\hat{\Psi}$ to be linear in r, $\hat{\Psi} = Ar$, and $\hat{\phi}$ takes the form

$$\hat{\phi}(r) = BJ_1(kr) - (k_B^2/k^2)Ar; \quad k = \omega/c.$$

Boundary conditions (4.15) require

$$\hat{\phi}'(R) = 0; \quad \hat{\phi}(R) = \mathrm{j}RA,$$

which yields the dispersion relation

$$k_B^2 J_2(kR) = \mathrm{j}k^2 J_1'(kR).$$

This requires that k is complex, and the waves are unstable for all non-zero k_B. The key point, though, is that the interface near marginal stability is of the form

$$\eta \sim J_1(kr)\sin(\theta - \omega t),$$

which represents a rotating, tilted interface. This is precisely what is expected from the compound pendulum analogue and is in accordance with our energy criterion.

6. A Fourier description of the motion

In this section, we show that our shallow-water equation (4.12) is equivalent to the mode-by-mode analysis of SW94 in the limit of small kh. We do this by expanding $\boldsymbol{q}_P$ in modes and then rewriting (4.12) in matrix form. Our motivation is partially to show that our analysis is consistent with the previous studies and partially because some results (particularly those relating to the stability threshold) are more readily obtained using the matrix formulation.

6.1. *A matrix formulation of the wave equation*

Following SW94, we start by expanding $\boldsymbol{q}_P$ in a set of orthogonal functions ψ_i defined by the eigenvalue problem

$$\nabla^2\psi_i + (\omega_{gi}/c)^2\psi_i = 0; \quad \nabla\psi_i \cdot \boldsymbol{n} = 0 \quad \text{on} \quad S. \tag{6.1}$$

We use ψ_i to represent the velocity potential of $\boldsymbol{q}_P$ and write

$$\boldsymbol{q}_P = \sum \boldsymbol{q}_i = \sum k_i^{-1} x_i(t)\nabla\psi_i.$$

Here $x_i(t)$ are the amplitudes of the modes and the factor k_i^{-1} is introduced to simplify the subsequent algebra. Of course, ψ_i are just the gravitational modes in the absence of Lorentz forces, and k_i and ω_{gi} are the corresponding wavenumbers and frequencies.

We now take the dot-product of (4.12) and $\nabla\psi_i$ and integrate over V. The result is

$$\ddot{x}_i(t) + \omega_{gi}^2 x_i = \omega_B^2 \sum K_{ij} x_j, \tag{6.2}$$

where the interaction matrix K_{ij} has elements

$$k_i k_j K_{ij} = \int (\nabla\psi_j \times \nabla\psi_i)_z \mathrm{d}V. \tag{6.3}$$

Here we have normalized ψ_i such that

$$\int \psi_i^2 \mathrm{d}V = 1.$$

Note that K_{ij} is skew-symmetric and has all of its diagonal elements equal to zero.

For the particular case of a rectangular cell of dimensions (L_x, L_y), the modes are simple cosines:

$$\psi_i = \psi_{mn} \sim \cos(m\pi x/L_x)\cos(n\pi y/L_y),$$
$$k_i^2 = k_{mn}^2 = (m\pi/L_x)^2 + (n\pi/L_y)^2.$$

The corresponding interaction matrix is

$$K_{mn,m'n'} = \frac{16\Delta_{mn,m'n'}}{L_x L_y k_{mn} k_{m'n'}}, \tag{6.4}$$

where

$$8\Delta_{mn,m'n'} = [m'(n+n')\delta_{n+n'}(\delta_{m+m'} - \delta_{m-m'}) \\ -n'(m+m')\delta_{m+m'}(\delta_{n+n'} - \delta_{n-n'})] \tag{6.5}$$

and δ_r is defined as $2/r$ if r is odd and zero if r is even. Equations (6.2) and (6.4) are equivalent to those of SW94 in the limit of small kH.

We now truncate x_i at some suitably small wavenumber and rewrite (6.2) in matrix form:

$$\ddot{\boldsymbol{x}} + \boldsymbol{\Omega}_g \boldsymbol{x} = \omega_B^2 \boldsymbol{K} \boldsymbol{x}. \tag{6.6}$$

This truncation is the primary weakness of the matrix formulation. We might try to defend this on the basis of the fact that, in reality, friction damps out the high-$\boldsymbol{k}$ waves. However, we require an inviscid theory which is self-consistent, so we must always check that the observed instabilities are independent of the number of modes used. We shall see in §7 that around 15 modes are sufficient to capture the behaviour of the large-wavelength instabilities. The effect of introducing more modes is not to change the predicted behaviour of the small-k instabilities, but rather to introduce additional unstable modes with smaller wavelengths. In addition, it might be argued that these small-wavelength perturbations are more susceptible to being damped out by friction. Consequently, truncation seems physically reasonable provided one is interested only in the long-wavelength behaviour.

6.2. *General behaviour of the matrix equations*

Consider the case where ω_B is much greater than the gravitational frequencies of the truncated system. In this case, (6.6) gives

$$\frac{\mathrm{d}^4 \boldsymbol{x}}{\mathrm{d}t^4} = -\omega_B^4 \boldsymbol{S}_1 \boldsymbol{x}; \quad \boldsymbol{S}_1 = -\boldsymbol{K}\boldsymbol{K}. \tag{6.7}$$

The equivalent eigenvalue problem is

$$\boldsymbol{S}_1 \boldsymbol{x} = -(\omega/\omega_B)^4 \boldsymbol{x} = \lambda \boldsymbol{x}. \tag{6.8}$$

Now $\boldsymbol{S}_1$ is real, symmetric and has positive diagonal elements. It follows that the eigenvalues, λ_i, are real and at least some of them are positive. We conclude, therefore, that for large ω_B at least some frequencies of our truncated system are complex.

Let us now return to the general eigenvalue problem represented by (6.6):

$$(\boldsymbol{\Omega}_g - \omega_B^2 \boldsymbol{K})\boldsymbol{x} = \lambda \boldsymbol{x}; \quad \lambda = \omega^2. \tag{6.9}$$

Suppose that $\boldsymbol{x}$ is truncated after N modes and that the diagonal elements of $\boldsymbol{\Omega}_g$ are arranged in order of increasing frequency, from ω_{g1}^2 to ω_{gN}^2. Then we may show that in the truncated system the eigenvalues, λ_i, have the following general properties:

(*a*) $\omega_{g1}^2 \leqslant \mathrm{Re}(\lambda) \leqslant \omega_{gN}^2$;

(*b*) $\sum \lambda_i = \sum \omega_{gi}^2$;

(*c*) λ_i/ω_B^2 are zero or purely complex if $\omega_B^2 \gg \omega_{gN}^2$.

These properties are sufficient to define the general behaviour of λ. The first follows from the skew-symmetry of $\boldsymbol{K}$. That is, if $\bar{x}_i$ is the complex conjugate of x_i, then

$$\sum_i (\omega_{gi}^2 - \lambda)|x_i|^2 = \omega_B^2 \sum_i \sum_j K_{ij} x_j \bar{x}_i.$$

If we normalize the eigenvectors to have unit magnitude and take the complex conjugate of the transpose of this equation, we obtain

$$\mathrm{Re}(\lambda) = \sum \omega_{gi}^2 |x_i|^2.$$

Condition (*a*) then follows. Condition (*b*), on the other hand, arises from the fact that the sum of the eigenvalues equals the trace of $\boldsymbol{\Omega}_g - \omega_B^2 \boldsymbol{K}$, while condition (*c*) is a standard result for skew-symmetric matrices.

The situation is therefore clear. As ω_B is increased, the eigenvalues move along the real axis but remain within the limits $\omega_{g1}^2 < \lambda < \omega_{gN}^2$. At some critical value of ω_B, two or more eigenvalues become complex (an inevitable consequence of condition (*c*)) and do so in the form of complex conjugate pairs (condition (*b*)). However, the real part of the complex eigenvalues remain bounded by the least and largest gravitational frequency of the truncated set of modes (condition (*a*)). Of course, this is precisely what is observed in the numerical solutions of SW94 and of BR94 and in the examples which follow.

7. Stability thresholds and a new stability criterion

The question of the threshold of stability was tackled in two different ways in SW94 and BR94. The first and most obvious route is to solve the general eigenvalue problem defined by (6.9). A second and simpler approach, emphasized particularly in SW94, is to look at the two modes which have the closest gravitational frequencies and reduce (6.9) to a 2×2 equation involving only those modes. This results in a simple analytical criterion for the onset of instability. This works well if there are two and only two modes with close natural frequencies. (Such modes interact with each other but not with the other modes.) It is not reliable if the initial frequencies, ω_{gi}^2, are uniformly dispersed along the real axis or if they are grouped in clusters composed of more than two frequencies.

The main purpose of this section is to show that there is a third approach to stability, which furnishes a sufficient condition for stability without the need to solve the eigenvalue problem (6.9). First, however, we consider briefly a simple set of numerical examples which illustrate a number of useful and unexpected results.

7.1. *Example of stability in a rectangular domain*

We now present a sequence of simple numerical examples which illustrate the phenomenon. We shall show that, frequently, it is not the pair of modes with the closest gravitational frequencies which go unstable first. Moreover, the modes which go unstable at the lowest value of $J_0 B_z$ need not be the most dangerous. Often the highest

growth rates are observed in the pairs of modes which are the second or third to go unstable. Of course, it is the modes with the highest growth rates which are most likely to survive the friction which is inevitably present in any real flow. Finally, we shall see that the truncation of the modes is not a severe problem and that, as observed in SW94, around 15 modes is sufficient to capture the behaviour of the long-wavelength instabilities.

Note that, since friction is absent from our model, the stability threshold will depend on the number of modes included in our analysis. That is, the threshold value of ω_B will depend on the minimum separation of the closest interacting gravitational frequencies. As the number of modes tends to infinity, this threshold will tend to zero. Of course, in practice only the long waves survive the friction present in the cell, and so in reality there is a cut-off in wavenumber. (Typically, only the first five modes are seen in a real cell.) Consequently, we shall focus only on the instability of the first few modes, but include higher wavenumbers in our analysis to ensure that truncation does not cause numerical errors in our long-wavelength predictions.

For simplicity, we confine ourselves to a rectangular domain. Many reduction cells have aspect ratios, L_x/L_y, in the range 0.3–0.4, and we consider both values. We start by rewriting (6.9) in dimensionless form. We use $k_1 = \pi/L_y$ as a characteristic (inverse) lengthscale and introduce

$$\hat{k}_i = k_i/k_1; \quad \hat{\lambda} = \omega^2/(ck_1)^2,$$

and

$$\epsilon = \left(\frac{2L_y}{\pi}\right)^4 \frac{J_0 B_z}{\Delta\rho g h H L_x L_y} = \left(\frac{2L_y}{\pi}\right)^4 \frac{\omega_B^2}{c^2 L_x L_y}.$$

Our matrix equation (6.9) then becomes

$$\hat{k}_i^2 x_i - \epsilon \sum_j k_i^{-1} k_j^{-1} \Delta_{ij} x_j = \hat{\lambda} x_i, \tag{7.1}$$

where Δ_{ij} is defined by (6.5). (There is no implied summation in the first term.) Note that each mode is characterized by two integers, (m, n), as shown in §6.1.

We consider first the case of $L_y/L_x = 0.3$. The trajectories of the eigenvalues in the complex plane are shown in figure 7 where the dots mark eigenvalues computed at constant intervals of ϵ and the stars represent the initial position of the eigenvalues (at $\epsilon = 0$). Three ranges of ϵ are indicated, corresponding to $\epsilon < 0.12$, $\epsilon < 0.15$, and $\epsilon < 0.20$. Figure 7(*a*) shows that, by $\epsilon = 0.12$, one pair of eigenvalues has coalesced and moved into the complex plane. In fact, these complex eigenvalues first appear at $\epsilon = 0.0577$, through the interaction of the (3,0) and (0,1) modes. (We classify the eigenvalues in terms of their mode number (m, n) when $\epsilon = 0$.) By $\epsilon = 0.15$, the complex eigenvalues have returned to the real axis and a new pair of unstable frequencies have appeared. This arises from an interaction of a (2,0) mode with one of the pair of previously unstable eigenvalues. By $\epsilon = 0.2$, two additional unstable pairs have appeared. One arises from the interaction of (1,1) and (2,1) modes, and the other through the interaction of the (1,0) mode with the second of the pair of previously unstable modes. We summarize the behaviour in table 1.

This simple example exhibits several interesting features. First, it is not the modes with the closest gravitational frequencies ω_{gi} which go unstable. In fact, the closest gravitational frequencies are the (0,1) and (1,1) modes, yet at no time do they combine to produce an instability. Second, by $\epsilon = 0.2$, the largest growth rate is exhibited not by the first instability, but by the fourth one. Given that any real flow has dissipation,

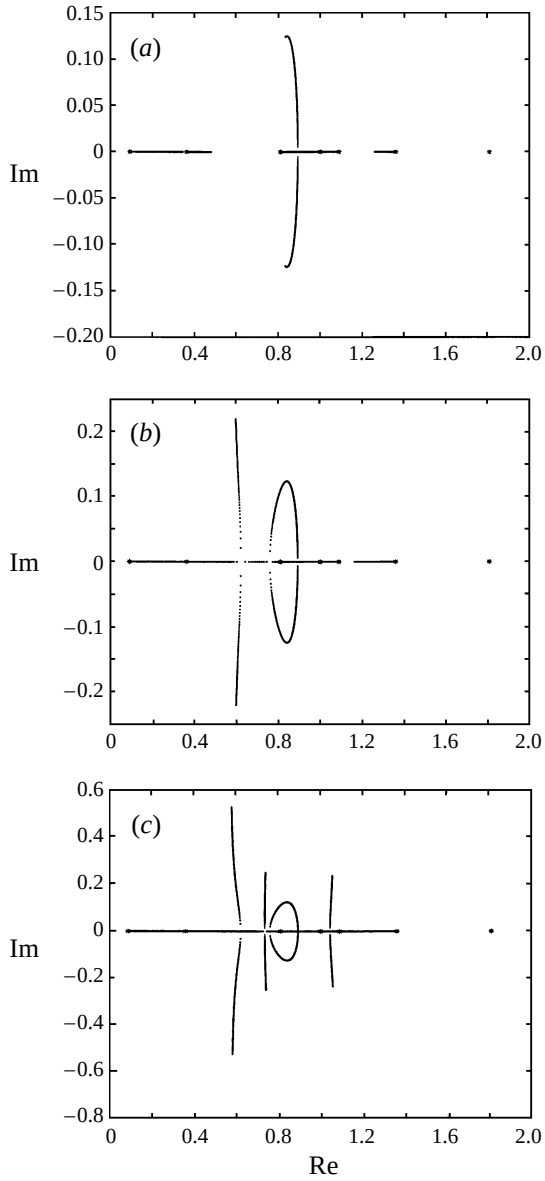

FIGURE 7. The trajectories of the eigenvalues in the complex plane with $L_y/L_x = 0.3$ and (*a*) $\epsilon_{max} = 0.12$, (*b*) $\epsilon_{max} = 0.15$, and (*c*) $\epsilon_{max} = 0.2$.

Instability	Modes	Comments
First	(3,0) + (0,1)	Restabilizes
Second	(2,0) + $\frac{1}{2}$ [(3,0) + (0,1)]	—
Third	(1,1) + (2,1)	Furthest to the right
Fourth	(1,0) + $\frac{1}{2}$ [(3,0) + (0,1)]	Furthest to the left

TABLE 1. Summary of unstable mode interactions with $L_y/L_x = 0.3$.

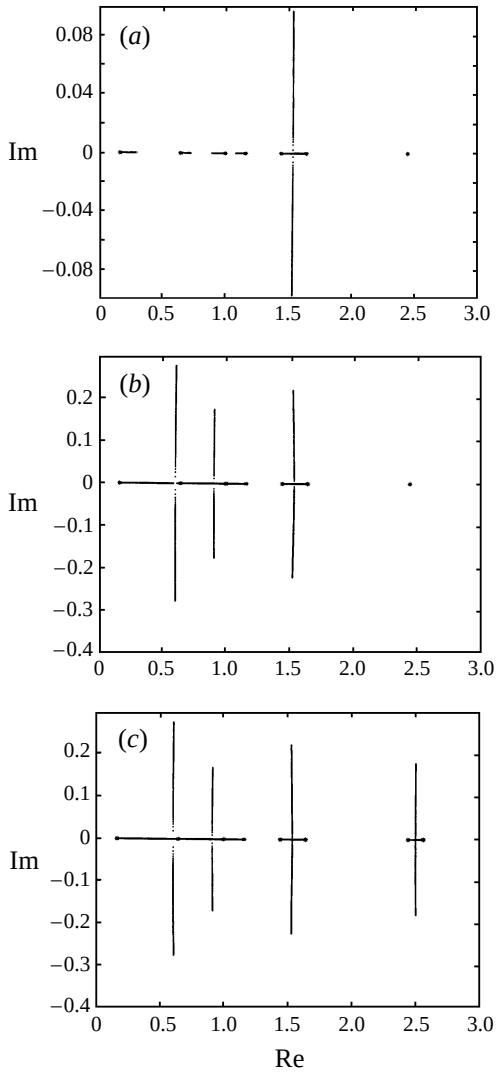

FIGURE 8. The trajectories of the eigenvalues in the complex plane with $L_y/L_x = 0.4$ and (*a*) $\epsilon_{max} = 0.12$, (*b*) $\epsilon_{max} = 0.2$, and (*c*) repeat of (*b*) for 63 modes.

it is this last instability which is the most likely to appear in practice. Third, if we had tried to capture the first instability by throwing out of (7.1) all of the modes except for (3,0) and (0,1), then we would have predicted an instability at $\epsilon = 0.0855$, which represents an error of 48%. This indicates that more than just two modes are interacting to produce the instability.

The case of $L_y/L_x = 0.4$ is shown in figure 8, for the ranges $\epsilon < 0.12$ and $\epsilon < 0.2$. This time the instabilities exhibit a simpler behaviour and appear in the order shown below (table 2). Once again, it is not the closest gravitational frequencies which lead to the first instability. Nor is it the first instability which ultimately has the highest growth rate. In fact, it is the third to appear.

Notice that in both examples, the first instability appears at quite low values of ϵ: $\epsilon = 0.0577$ ($\omega_B L_y/c = 1.08$) in the first case and $\epsilon = 0.0875$ ($\omega_B L_y/c = 1.15$) in the second. This low threshold is in line with the predictions of SW94 and BR94, who

Instability	Modes	Comments
First	(3,0) + (2,1)	Furthest to the right
Second	(0,1) + (1,1)	—
Third	(1,0) + (2,0)	Furthest to the left

TABLE 2. Summary of unstable mode interactions with $L_y/L_x = 0.4$.

Number of modes, N	Critical ϵ	Unstable mode pairs
15	0.0878	(3,0) + (2,1)
63	0.0875	(3,0) + (2,1)
	0.0649	(3,1) + (4,0)
224	0.0875	(3,0) + (2,1)
	0.0648	(3,1) + (4,0)
	0.0608	(9,2) + (10,1)

TABLE 3. The effect of truncation on the predicted unstable mode pairs with $L_y/L_x = 0.4$ and $\epsilon < 0.1$.

note that an instability may result for quite modest values of ω_B^2 if two values of ω_{gi}^2 are particularly close. The idea is that, while ω_B is still quite small, two adjacent frequencies might interact, converge, and move off into the complex plane. If the initial frequencies are close, this interaction is a local one, in the sense that it does not involve the other modes. This, in turn, leads to the idea that modes with close gravitational frequencies are dangerous. However, it is important to note that $\boldsymbol{K}$ is very sparse. For example, in a rectangular cell $\Delta_{mn,m'n'}$ is zero for most combinations of (m,n) and (m',n'). Indeed only around one in five mode-pairs are coupled. In general, then, relatively few modes exchange energy. It is not difficult to show that an instability cannot develop from these uncoupled modes, so it is only the separation of the coupled modes which is important. Thus a stability criterion based on keeping all gravitational modes apart is overly conservative. This point is of considerable practical importance and is clearly illustrated in the previous examples.

We conclude this section with a discussion of truncation error. The previous results were obtained using 15 modes. Consider the case of $L_y/L_x = 0.4$ and $\epsilon < 0.1$. If we increase the number of modes to first 63 and then 225, we obtain the following. (See table 3.)

The effect of increasing N is to introduce additional unstable modes at lower critical values of ϵ and with higher wavenumbers. However, the prediction of the longest wavelength instability is unchanged. This is illustrated by figure 8(c) where the calculation of figure 8(b) is repeated using 63 rather than 15 modes. Comparing 8(b) and 8(c), we see that the behaviour of the first three unstable modes is initially identical for 15-mode and 63-mode truncation. The effect of adding more modes is simply to trigger additional high-wavenumber instabilities. Since the high-k waves are likely to be damped out by friction, truncation does not seem to be a problem, which is exactly what SW94 concluded.

7.2. *A new stability criterion*

In conclusion, we derive a sufficient condition for stability based on Gershgorin's theorem. We start with (6.9):

$$\left(\boldsymbol{\Omega}_g - \omega_B^2 \boldsymbol{K}\right) \boldsymbol{x} = \omega^2 \boldsymbol{x}.$$

Gershgorin's theorem links each eigenvalue to one of the diagonal elements of $\boldsymbol{\Omega}_g$ and places bounds on the separation of ω_i^2 and ω_{gi}^2 in the complex plane. That is,

$$\left|\omega_i^2 - \omega_{gi}^2\right| \leqslant \omega_B^2 \sum_{p=1}^{N} |K_{ip}| \,. \tag{7.2}$$

Now suppose ω_{gi}^2 and ω_{gj}^2 are the closest gravitational frequencies of our truncated system. Then the frequencies ω_i^2 and ω_j^2 cannot meet on the real axis if their initial separation exceeds the sum of the bounds $\omega_B^2 b_i$ and $\omega_B^2 b_j$, where $b_i = \sum |K_{ip}|$. Thus, the interface is stable (with respect to our truncated set of modes) provided

$$\left|\omega_{gi}^2 - \omega_{gj}^2\right| > \omega_B^2 \left(b_i + b_j\right).$$

We conclude, therefore, that a sufficient condition for stability is

$$\frac{J_0 B_z}{\bar{\rho} h H} < \frac{\left|\omega_{gi}^2 - \omega_{gj}^2\right|}{\left(b_i + b_j\right)}. \tag{7.3}$$

The value of (7.3) is that we need not solve the eigenvalue problem (6.9). It is only necessary to add the elements of the appropriate columns of the interaction matrix, $\boldsymbol{K}$, to obtain the bounds b_i and b_j. It is interesting to compare (7.3) with (3.3) for the compound pendulum. The two are very similar.

Conclusions

We have shown that a wave equation for the interface in aluminium reduction cells can be developed from shallow-water theory. Our approach involves expressing the Lorentz force directly in terms of the velocity and is more general than previous formulations. The new equation is valid regardless of the existence or form of boundaries. In the case of rectangular lateral boundaries, the model leads to the (potentially unstable) standing waves of SW94. For circular domains, a particularly simple form of instability is found. When an infinitely long channel is considered, we discover a new set of unstable travelling waves.

When the equation is expressed in matrix form, in the manner of SW94, we obtain some unexpected results. It is frequently not the pair of modes with the closest gravitational frequencies which first become unstable. Also, the largest growth rate is not necessarily observed in the first unstable mode-pair. Perhaps the two most important points are that, for rectangular domains, relatively few mode-pairs are coupled and the uncoupled pairs cannot become unstable.

We have derived a sufficient condition for stability which does not require us to solve the equations of motion explicitly. The use of Gershgorin's theorem enables us to place a lower bound on the critical value of the background magnetic field at which an instability first appears.

REFERENCES

Bojarevics, V. & Romerio, M. V. 1994 Long waves instability of liquid metal-electrolyte interface in aluminium electrolysis cells: a generalization of Sele's criterion. *Eur. J. Mech.* B **13**, 33–56 (referred to herein as BR94).

Davidson, P. A. 1994 An energy analysis of unstable, aluminium reduction cells. *Eur. J. Mech.* B **13**, 15–32.

MOREAU, R. J. & ZIEGLER, D. 1986 Stability of aluminium cells: a new approach. *Light Metals*, pp. 359–364.

PEDLOSKY, J. 1979 *Geophysical Fluid Dynamics*. Springer.

PIGNY, S. & MOREAU, R. 1992 Stability of fluid interfaces carrying a electric current in the presence of a magnetic field. *Eur. J. Mech.* B **11**, 1–20.

SEGATZ, M. & DROSTE, C. 1994 Analysis of magnetohydrodynamic instabilities in aluminium reduction cells. *Light Metals*, pp. 313–322.

SELE, T. 1977 Instabilities of the metal surface in electrolyte alumina reduction cells. *Metall. Trans.* B **8B**, 613–618.

SNEYD, A. D. 1985 Stability of fluid layers carrying a normal electric current. *J. Fluid Mech.* **156**, 223–236.

SNEYD, A. D. 1992 Interfacial instabilities in aluminium reduction cells. *J. Fluid Mech.* **236**, 111–126.

SNEYD, A. D. & WANG, A. 1994 Interfacial instability due to MHD Mode coupling in aluminium reduction cells. *J. Fluid Mech.* **263**, 343–359 (referred to herein as SW94).

URATA, N. 1985 Magnetics and metal pad instability. *Light Metals*, pp. 581–589.